

Investigation of feasibility of noise suppression method for cavitation-enhanced high-intensity focused ultrasound treatment

Ryo Takagi^{a,*}, Yoshihiko Koseki^a, Shin Yoshizawa^b, Shin-ichiro Umemura^b

^a *Health and Medical Research Institute, National Institute of Advanced Industrial Science and Technology (AIST), Tsukuba 305-8564, Japan*

^b *Graduate School of Engineering, Tohoku University, Sendai 980-8579, Japan*



ARTICLE INFO

Keywords:

High-intensity focused ultrasound
Cavitation
Ultrasound imaging
Noise suppression

ABSTRACT

In high-intensity focused ultrasound (HIFU) treatment, a method that monitors tissue changes while irradiating therapeutic ultrasound is needed to detect changes in the order of milliseconds due to thermal coagulation and the presence of cavitation bubbles. The new filtering method in which only the HIFU noise was reduced while the tissue signals remained intact was proposed in the conventional HIFU exposure in our preliminary study. However, HIFU was irradiated perpendicular to the direction of the imaging ultrasound in the preliminary experiment, which was believed to be impractical. This study investigated the efficacy of the proposed method a parallel setup, in which both HIFU and imaging beams have the same axis just as in a practical application. In addition, this filtering algorithm was applied to the "Trigger HIFU" sequence in which ultrasound-induced cavitation bubbles were generated in the HIFU focal region to enhance heating. In this setup and sequence, HIFU noise level was increased and the summation or difference tone induced by the interaction of HIFU waves with the imaging pulse has the potential to affect this proposed method. Ex-vivo experiments proved that the HIFU noise was selectively eliminated by the proposed filtering method in which chaotic acoustic signals were emitted by the cavitation bubbles at the HIFU focus. These results suggest that the proposed method was practically efficient for monitoring tissue changes in HIFU-induced cavitation bubbles.

1. Introduction

In high-intensity focused ultrasound (HIFU) treatment, ultrasound is exposed from outside the body and focused typically at a cancerous tissue, enabling selective treatment of tissue through thermal coagulation [1-4]. HIFU treatment is non-invasive compared with the surgical operation and has been clinically used for more than a decade [5-9]. Despite this advantage, HIFU has a long treatment time of typically 1–3 h due to the required cooling period to avoid undesirably heating intervening normal tissues such as the skin. To shorten the treatment time, a method with enhanced efficiency needs to be developed. Real-time monitoring of HIFU treatment is also needed to enable accurate feedback regarding the changes in tissue during HIFU exposure. Magnetic Resonance Imaging (MRI) [10,11] and ultrasound imaging [5,12,13] have been the two popular means of this. This study prefers to use ultrasonic imaging because of its relatively low cost and ability to acquire images with high temporal resolution [14,15].

Some methods using ultrasound have been investigated to characterize thermal change induced by HIFU exposure. Simon et al. suggested

to estimate the temperature increase from the echo shift during HIFU exposure [16]. Techniques using the acoustic radiation force impulse (ARFI) and shear wave imaging have been studied to estimate the elasticity of tissues [17-20].

Some methods have been suggested for detecting changes in ultrasonic backscatter in real-time for visualizing the thermal coagulation induced by HIFU [21-24].

To achieve real-time ultrasonic imaging during HIFU treatment, it is necessary to combine the HIFU transducer with an ultrasound imaging probe. However, the quality of the ultrasound images would be severely corrupted by the reflected HIFU signal if the HIFU transducer and imaging probe were simultaneously activated. Several methods have thus been developed and used to obtain interference-free B-mode images.

The most facile method to obtain ultrasonic images without HIFU noise is to set the interval for imaging between HIFU bursts [25,26]. The temporal resolution for monitoring treatment using this method has been limited.

A few methods to reduce the HIFU noise from the RF signals received by the ultrasonic probe without the intervals for imaging have been

* Corresponding author.

E-mail address: ryo-takagi@aist.go.jp (R. Takagi).

proposed to improve the temporal resolution. Jeong et al. suggested a method in which a long-burst HIFU for treatment and a chirp sequence for imaging are transmitted simultaneously and the HIFU noise is suppressed using notch filters [27]. They also suggested another method using traditional short-pulse excitation with adaptive notch filters to cancel the HIFU noise [28]. The concept of these methods is basically to eliminate the HIFU noise using a frequency-domain filter, which reduces the components of both HIFU noise and the tissue echo signals.

Song et al. suggested that the application of a pulse inversion sequence to the HIFU exposure to suppress the fundamental and odd harmonic components of the HIFU interference received by the imaging probe to obtain B-mode images without HIFU noise [29]. This method is considered to be effective in a situation, where the frequency band for imaging does not overlap the second harmonic components of the HIFU.

Herein we have proposed a novel and facile method to reduce only the components of HIFU in RF signals before dynamic focus processing [24]. This method assumes use of a coupling medium between the HIFU transducer and the tissue. The CW response of the tissue to HIFU exposure was estimated based on the RF signal of each channel of the imaging probe in the time period before the arrival of the pulse echo signals from the tissue. The estimated CW response was then subtracted from the received RF signal.

Our preliminary study [24] showed that the proposed method was able to reduce the only HIFU noise from the RF signals that were significantly contaminated with HIFU noise interference. However, HIFU was irradiated perpendicular to the direction of the imaging beam, which was very impractical.

In this study, the efficacy of the proposed method is investigated in a parallel setup, in which both HIFU and imaging beams have the same axis. This parallel setup is much more practical than the preliminary tested perpendicular setup. However, a significantly more HIFU noise will be received by the probe and the received signal may suffer much more from the effect of the summation or difference tone induced by the interaction of HIFU waves with the imaging pulse or its radiation force.

To improve the efficiency of the HIFU treatment, we have focused our attention on utilizing the cavitation bubbles induced by HIFU [25]–[27]. The bubbles are known to enhance the heating effect of ultrasound during HIFU exposure because the acoustic energy dissipation is increased by the volumetric oscillation of the cavitation bubbles [28,29]. In another preliminary study of ours, the ultrasound sequence, named “Trigger HIFU”, consisting of high-intensity short-bursts followed by relatively low-intensity continuous waves was proposed and used to enlarge the coagulation region [30]–[33]. In this study, the proposed method was also tested in the case of cavitation-enhanced HIFU treatment (“Trigger HIFU” sequence), where the HIFU noise may have more transient components and higher amplitudes than those of the conventional HIFU treatment.

2. Materials and methods

2.1. Experimental setup

Fig. 1 shows a schematic of the experimental setup. In contrast with the previous study, the imaging probe was set inside the therapeutic transducer so that the direction of the imaging ultrasound was parallel to that of the HIFU exposure. HIFU was exposed from a 1–3 piezocomposite concentric-ring transducer of high fill-factor as shown in **Fig. 2**[24,34] (Imasonic, Voray sur l’Ognon, France). The transducer had 256 with equal area of 134 mm² elements. The adjacent pairs of these elements were electrically combined to virtually form the 128-element phased array transducer to drive the whole transducer with a limited number of amplifiers as shown in **Fig. 2**. The resonance frequency and radius of curvature of the transducer were 1.25 MHz and 120 mm respectively. This transducer with outer and inner diameters of 120 and 40 mm, respectively, was connected to staircase voltage drive amplifiers [35] (Microsonic, Tokyo, Japan) controlled by a PC and operated at 1.25 MHz. The –3dB focal width and length were 1.2 mm and 9.0 mm respectively [24]. A phased array probe with a center frequency of 3

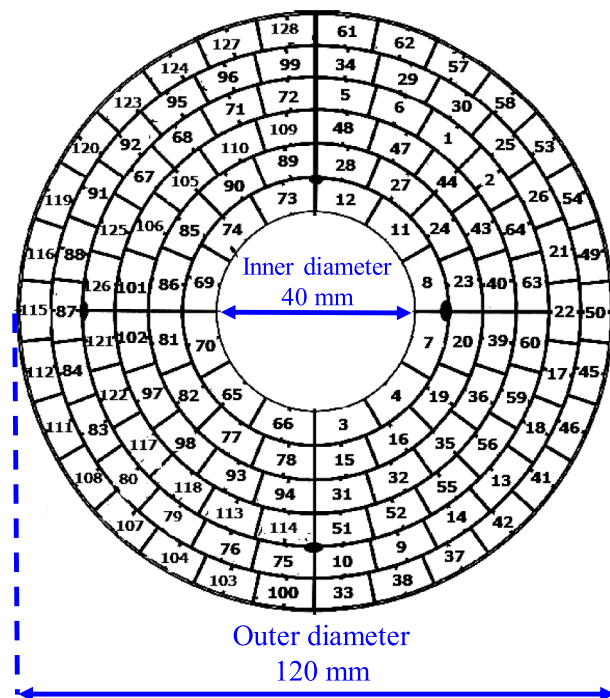


Fig. 2. Channel allocation of HIFU transducer.

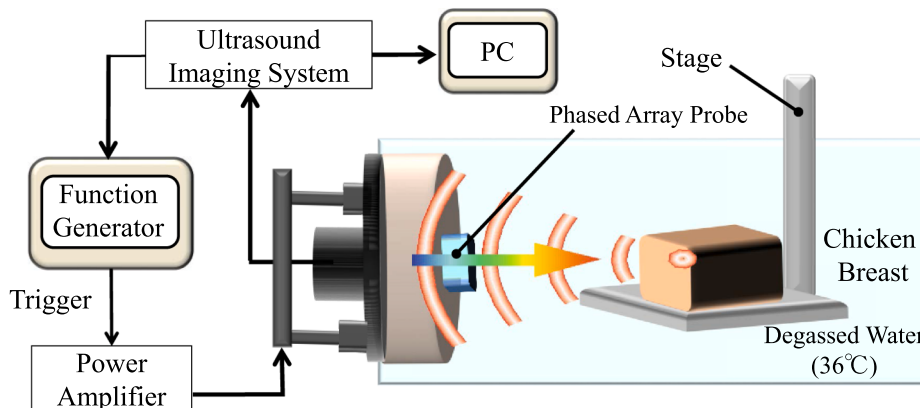


Fig. 1. Experimental setup.

MHz (UST-52105, Hitachi Aloka Medical, Tokyo, Japan) was mounted inside the therapeutic transducer so that the direction of the HIFU beam was parallel to that of the imaging beam. The mounted probe was used to receive the echo signals to generate B-mode images and to detect tissue changes. A freshly excised chicken breast was used as a sample tissue. The tissue was degassed in saline (0.09% by mass) for 3 h to decrease the amount of remaining gas in the tissue. The position of the tissue sample was fixed in the water tank so that the HIFU focus was localized 10–15 mm in depth from the surface of the tissue sample. The water in the tank was also degassed and kept at approximately 36°C.

2.2. HIFU exposure and data acquisition

Fig. 3 shows the “Heating only” and “Trigger HIFU” sequences of HIFU exposure with the timings of RF signal acquisition [30–33]. The upper (a) and lower (b) figures show the HIFU exposure sequences named “Heating only” and “Trigger HIFU” sequences, respectively [30–33]. The waveform of the “Trigger HIFU” has two components: an extremely high-intensity short pulse for generating cavitation bubbles (called the “trigger pulse”) and a relatively low-intensity long burst for heating through the vibrating cavitation bubbles (called “heating burst”). The heating effect of the “Trigger HIFU” sequence was confirmed in our previous studies [30–33]. In this study, the duration of the trigger pulse and the following heating burst was 50 µs and 200 ms, respectively. This sequence was repeated 50 times, resulting in a total duration of 10 s. The spatial-peak temporal-peak intensity (I_{SPTP}) of the trigger pulse and the heating burst was 30 and 2.0 kW/cm², respectively. These acoustic intensities were estimated based on the focal pressure measured in the water with a hydrophone (HGL-1313, Onda, Sunnyvale, CA, USA) at a low intensity level (1 W/cm²) by assuming a quadratic relation between the amplifier output voltage and the acoustic intensity.

The “Heating only” sequence had no trigger pulses and the total exposure time was the same as that of the “Trigger HIFU”. I_{SPTP} of the heating burst was 2.0 kW/cm². The HIFU exposure experiments using different tissue samples were repeated 5 times in the “Heating only” and “Trigger HIFU” sequences, respectively (10 times in total).

An ultrasound echography system (V-1 System, Verasonics, Redmond, WA, USA) and a phased-array probe (UST-52105, Hitachi Aloka Medical, Tokyo, Japan) with a center frequency of 3 MHz were used to acquire the ultrasonic RF signals. The phased array probe had 80 channels. The RF signals were obtained continuously at a rate of 25 Hz during the heating burst without HIFU intermission. The imaging plane was set so that it contained the axis of the HIFU. In this study, high-speed imaging by parallel beamforming was performed using the RF signals acquired during HIFU exposure. Seven plane wave pulses were transmitted with a separation of 6°. The RF signals were obtained in a form of In-phase and Quadrature (IQ) data and coherently compounded to enhance the contrast ratio of the B-mode images. The pulse repetition period between the transmitted pulses was 200 µs.

2.3. HIFU noise reduction algorithm

Basically, the same algorithm as the preliminary study [24] was used to reduce the HIFU noise in the practical setup in which the imaging probe was set inside the therapeutic transducer. An example of an RF signal received by an array element of the imaging probe is shown in **Fig. 4(a)** in the case of “Trigger HIFU” exposure. The horizontal and vertical axes in **Fig. 4** show time and amplitude, respectively. As shown in **Fig. 4(a)**, the RF signal contains both the continuous wave response to the HIFU waves [$CW(t)$] and the pulse response [$u(t)$]. The algorithm assumes that $CW(t)$ should reach a steady state in less than an order of a millisecond after the HIFU exposure starts [24], such that the response

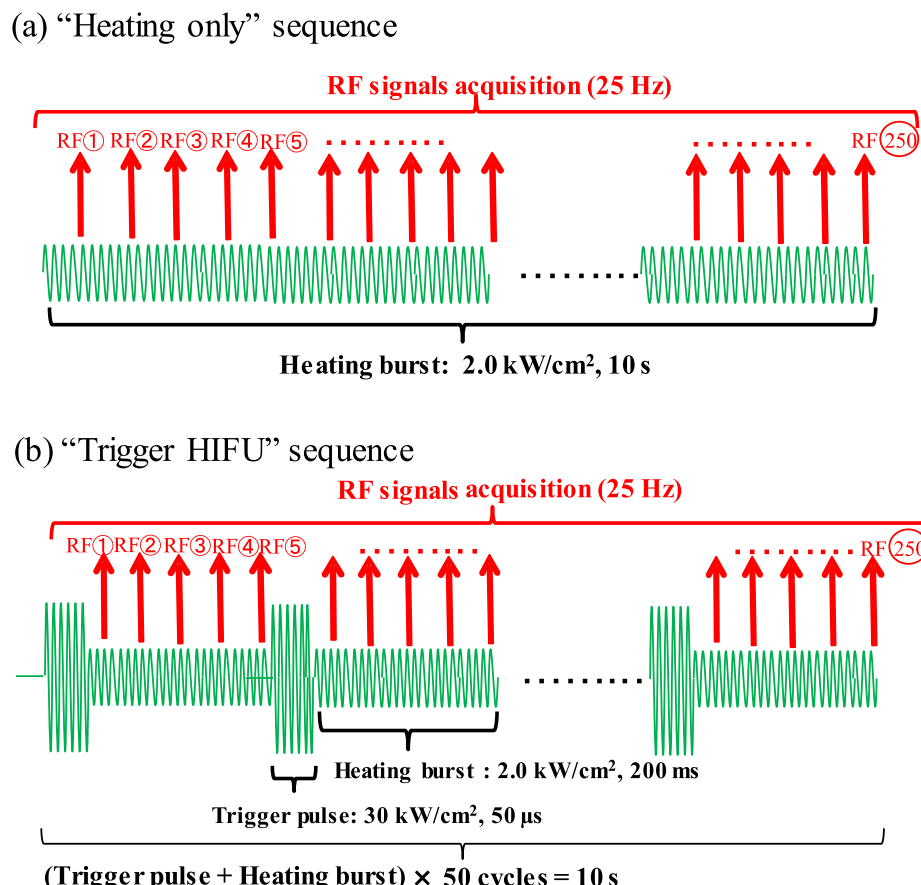


Fig. 3. Sequences of HIFU exposure with the timings of RF signal acquisition.

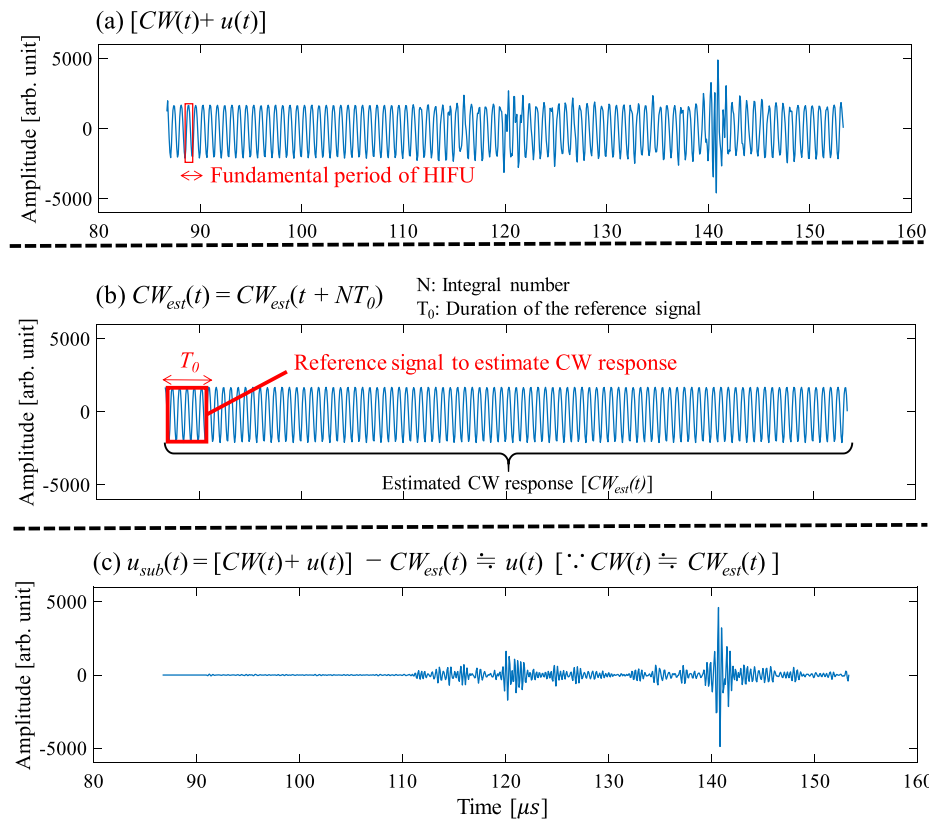


Fig. 4. Diagram of noise-reduction algorithm (an example of an RF signal received by an array element of the imaging probe).

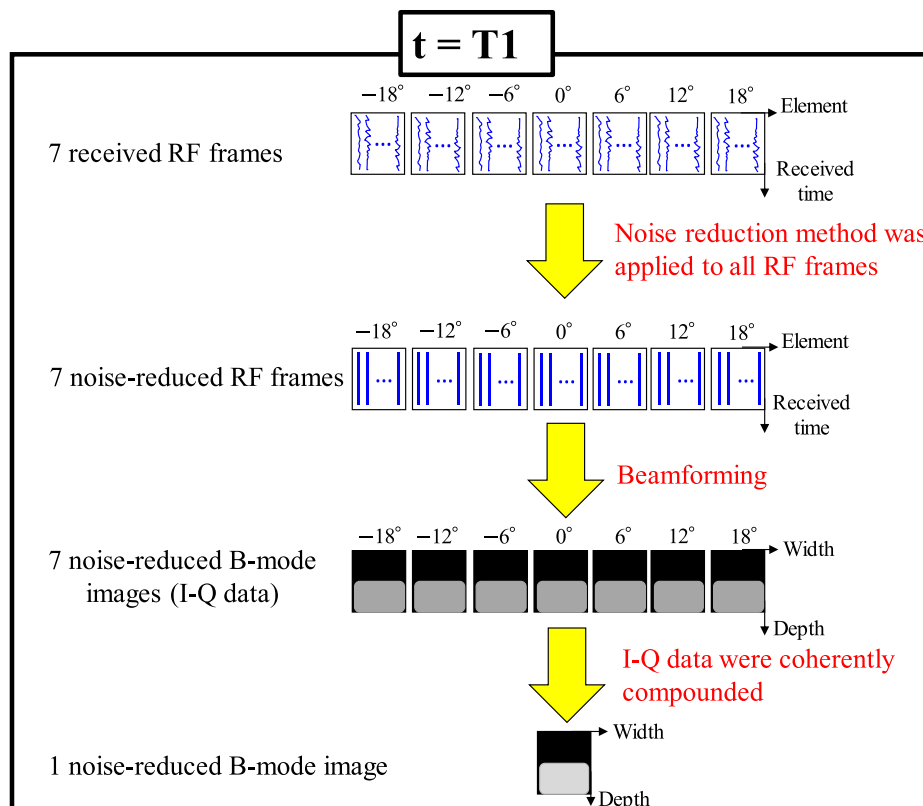


Fig. 5. Diagram of the proposed processing.

to the HIFU should be periodic with a period integer multiple of that of HIFU ($0.8 \mu\text{s}$ in this study). Therefore, the CW response [$CW_{est}(t)$] can be estimated using the RF signal in a time window that corresponds to the water region between the tissue (the pulse echo: $u(t)$) and the transducer and can extend to outside the time window assuming the periodicity of $CW_{est}(t)$, where

$$CW_{est}(t) = CW_{est}(t + NT_0) \quad (N = 0, \pm 1, \pm 2, \dots) \quad (1)$$

as shown in Fig. 4 (b). Here, N and T_0 are the integral number and reference signal duration, respectively. The actual time range of the reference signal was from 88 to $92 \mu\text{s}$ ($T_0 = 4 \mu\text{s}$). The estimated CW response, $CW_{est}(t)$, should be almost the same as the $CW(t)$ as long as $CW(t)$ is not seriously affected by a transient event such as cavitation, which occurs on a time scale of an order of microseconds. Under such a condition, the pulse response, $u(t)$, can be ascertained by subtracting $CW_{est}(t)$ from the entire RF signal [$CW(t) + u(t)$] described as

$$u_{sub}(t) = [CW(t) + u(t)] - CW_{est}(t) \approx u(t) \quad [: CW(t) \approx CW_{est}(t)] \quad (2)$$

as shown in Fig. 4 (c). Here, $u_{sub}(t)$ is the RF signal after the subtraction. The entire duration of the received RF signal in each element was about $80 \mu\text{s}$, as shown in Fig. 4. If $CW(t)$ is distorted and assumes a non-steady state because of an instantaneous tissue change such as cavitation, the $CW_{est}(t)$ is deviated from the $CW(t)$ and the noise remains in the RF signal after the subtraction ($u_{sub}(t)$).

Fig. 5 shows the diagram of the proposed processing. As described in Section 2.2, the seven RF signals received in each element (called “RF frames” in Fig. 5) were obtained at a rate of 25 Hz during HIFU exposure. At each time ($t = T_1$ in Fig. 5), the proposed method was applied to all seven RF frames to reduce the noise and seven B-mode images (IQ data) were acquired and coherently compounded to enhance the contrast ratio of the images.

It is important to control the preamplifier gain so that the level of RF signals fall inside the full range. A large dynamic range is needed to reduce the HIFU noise using this algorithm while maintaining the signal-to-noise ratio (S/N) of the obtained ultrasonic image. In this study, the full range of the receiver was 14 bits and proved to be sufficient to maintain the S/N, which was adequate for detecting the tissue changes due to HIFU-induced coagulation.

It should be noted that the proposed noise elimination, using the steady state CW response, must be applied to the received RF signals before (not after) the dynamically focused beamforming. This is because the phase of RF signals is modulated by the dynamic beamforming as a function of imaging depth and the HIFU response varies depending on the dynamic focal distance.

2.4. Analysis of the received RF signal

This study calculates the differences in the power frequency spectra between the RF signals before and after noise reduction to evaluate the

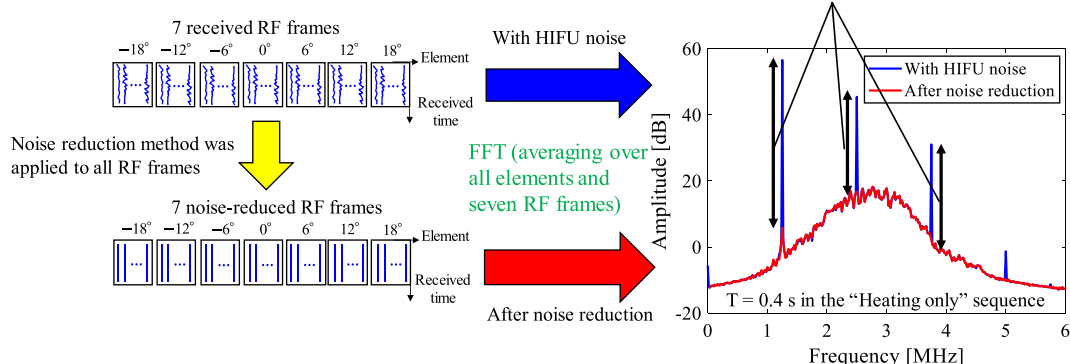


Fig. 6. Schematic diagram of the analysis of the received RF signal.

efficacy of the method in both the “Heating only” and “Trigger HIFU” sequences. Fast Fourier Transform (FFT) was applied to the 80-element received or processed RF signals and the frequency spectra were calculated and averaged over 80 elements and seven RF frames at each time.

The averaged RF signal power at the fundamental second and third component of HIFU (1.25 , 2.5 and 3.75 MHz , respectively) between the RF signal with and after reducing HIFU noise was calculated and referred to as the “noise reduction level”. It is thought that the noise reduction level decreases when the proposed method fails and the HIFU components remain in the noise-reduced RF signal. Fig. 6 shows the schematic diagram of the analysis of the received RF signal. An example of the averaged frequency spectra with HIFU noise and after noise reduction at 0.4 s after HIFU exposure (“Heating only” sequence) is also shown in Fig. 6.

2.5. Cross – correlation coefficient distribution

In the case of “Heating only” sequence, the cross-correlation algorithm was applied to the B-mode images after noise reduction using a method for detecting thermal coagulation as shown in our previous study [22,23]. Fig. 7 shows the diagram of the calculation of cross-correlation coefficient between reference and target frames (B-mode images) after noise reduction.

The correlation coefficient is calculated as

$$|R(k, l)| = \frac{\left| \sum_{i=1}^{M_i} \sum_{j=1}^{N_j} T^*(i, j) I(i+k, j+l) \right|}{\sqrt{\sum_{i=1}^{M_i} \sum_{j=1}^{N_j} |T(i, j)|^2} \sqrt{\sum_{i=1}^{M_i} \sum_{j=1}^{N_j} |I(i+k, j+l)|^2}} \quad (3)$$

($-M_k \leq k \leq M_k$, $-N_l \leq l \leq N_l$)

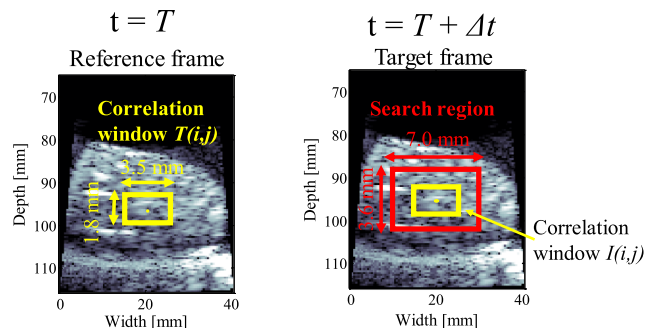
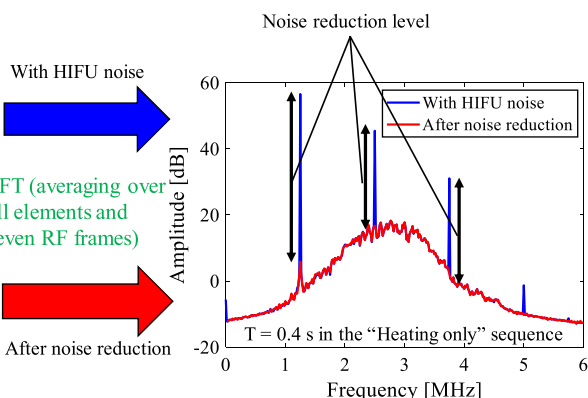


Fig. 7. Diagram of the calculation of cross-correlation coefficient between the reference and target frames (B-mode images) after noise reduction.



here, $T(i,j)$ denotes the B-mode image signals in a “correlation window”, set in a reference frame, and $I(i,j)$ denotes those in a window with the same size, which was searched in the target frame. The i and j parameters refer to the lateral (direction of width) and axial (direction of depth) position in the correlation windows ($T(i,j), I(i,j)$), respectively. As shown in Fig. 7, $T(i,j)$ was chosen as a reference window in a reference frame. The window $I(i,j)$ that matches the $T(i,j)$ was searched in a search region in the target frame. M_i and N_j in Eq. (3) indicate the lateral and axial length of the correlation window and that of the search region which are $2 \times M_k + 1$ and $2 \times M_l + 1$, respectively. The size of the correlation window and the search region was set to 3.5×1.8 mm (9×5 pixels) and 7.0×3.6 mm (17×9 pixels), respectively. This means that the parameters of M_i , N_j , M_k , and N_l were set to 9, 5, 8, and 4, respectively in Eq. (3). These values were determined considering the spatial resolution of the obtained distribution of correlation coefficient to clearly observe the decorrelation region that corresponds to the size of thermal coagulation [22]. The time between two B-mode images (Δt in Fig. 7) to calculate the cross-correlation coefficient was 200 ms in this study. The validity of these parameter settings was already confirmed by the preliminary study [22,23].

Once the correlation coefficients between two windows were calculated within the search region in the target frame at $T + \Delta t$ in Fig. 7, the maximum correlation coefficient

$$R_{max} = \max[R(k,l)] \quad (4)$$

was stored at the position of the reference frame at T in Fig. 7. The frame at $T + \Delta t$ in Fig. 7 was then set as the next reference frame. The cross-correlation coefficients were calculated between the next reference ($T + \Delta t$) and target frames ($T + 2 \times \Delta t$). This formed a motion-compensated similarity distribution between the two frames. The position of the nearest neighbor correlation windows in a reference frame was set such that they overlapped 50% to achieve a sufficient spatial resolution.

3. Results

3.1. The “Heating only” sequence

Fig. 8 (a) and (b) show the B-mode images during the “Heating only” sequence, before and after the HIFU noise reduction, respectively. Here, HIFU was irradiated from above in a downward direction. In this case, the reference RF signals used to estimate the entire CW response were those corresponding to a depth of around 70 mm in the B-mode images. The tissue image is clearly seen and the tissue change can be recognized in Fig. 8 (b) after the HIFU noise reduction. In contrast, the tissue image during HIFU exposure is almost fully contaminated with HIFU noise in Fig. 8 (a).

Fig. 9 shows the distributions of the correlation coefficient between the B-mode images in Fig. 8. The time distance between two frames to generate the distributions of the correlation coefficient was 40 ms in this experiment. A contiguous region with decreased correlation coefficients is seen near the HIFU focus in Fig. 9 (b) after the HIFU noise reduction. In contrast, they are not seen in Fig. 9 (a). In these maps, the coefficients in the region corresponding to the coupling water were deliberately set to zero by automatically detecting the boundary between the tissue and the water.

To compare with the ultrasonically detected actual coagulation region (photographs), the distributions of correlation coefficient and photographs after HIFU exposure were binarized. Fig. 10 (a) shows a binarized distribution of the correlation coefficient in the focal region, where the region that is less than 0.95 of the correlation coefficient was kept as the white region. Fig. 10 (b) shows a binarized photography of a cross-sectional slice of tissue sample after HIFU exposure. The axial and lateral length of the focal region were defined as “Major diameter” and “Minor diameter” from the binarized images in Fig. 10 (a) and (b). The area of coagulation was estimated using the following equation.

$$(Area of coagulation) = \pi \times \frac{(\text{Major diameter})}{2} \times \frac{(\text{Minor diameter})}{2} \quad (5)$$

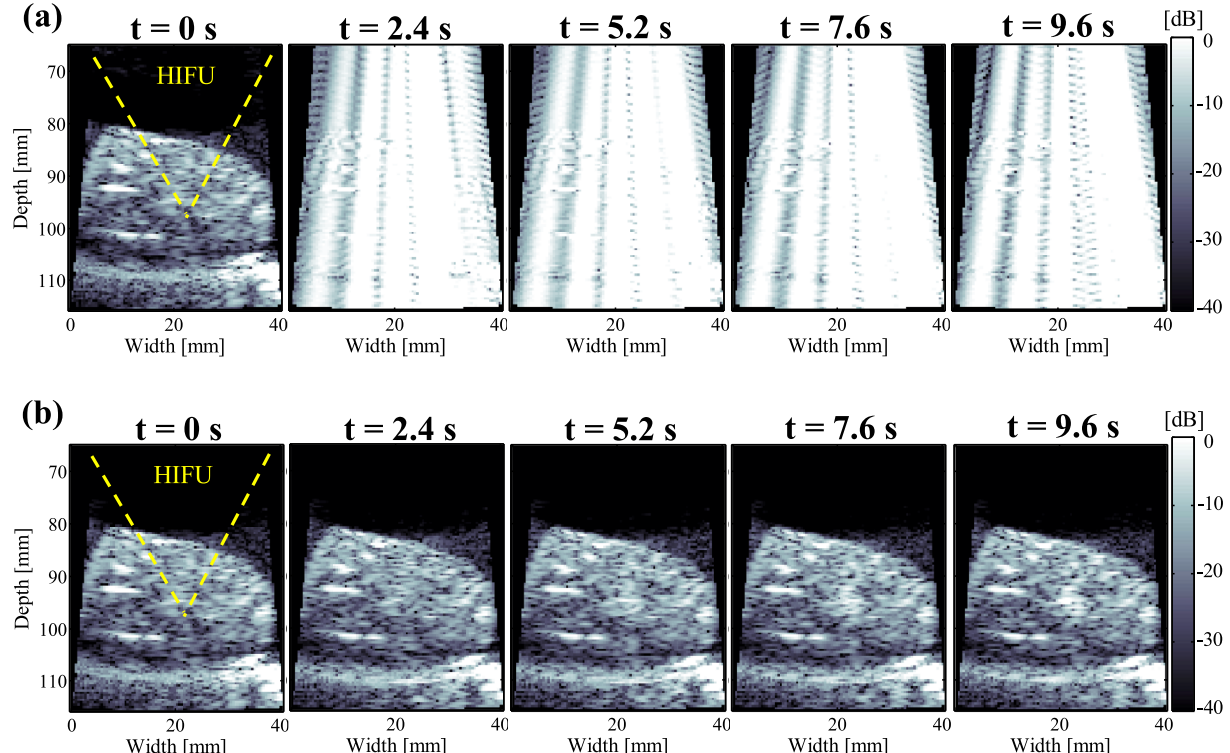


Fig. 8. B-mode images during the “Heating only” sequence (a) before and (b) after HIFU noise reduction.

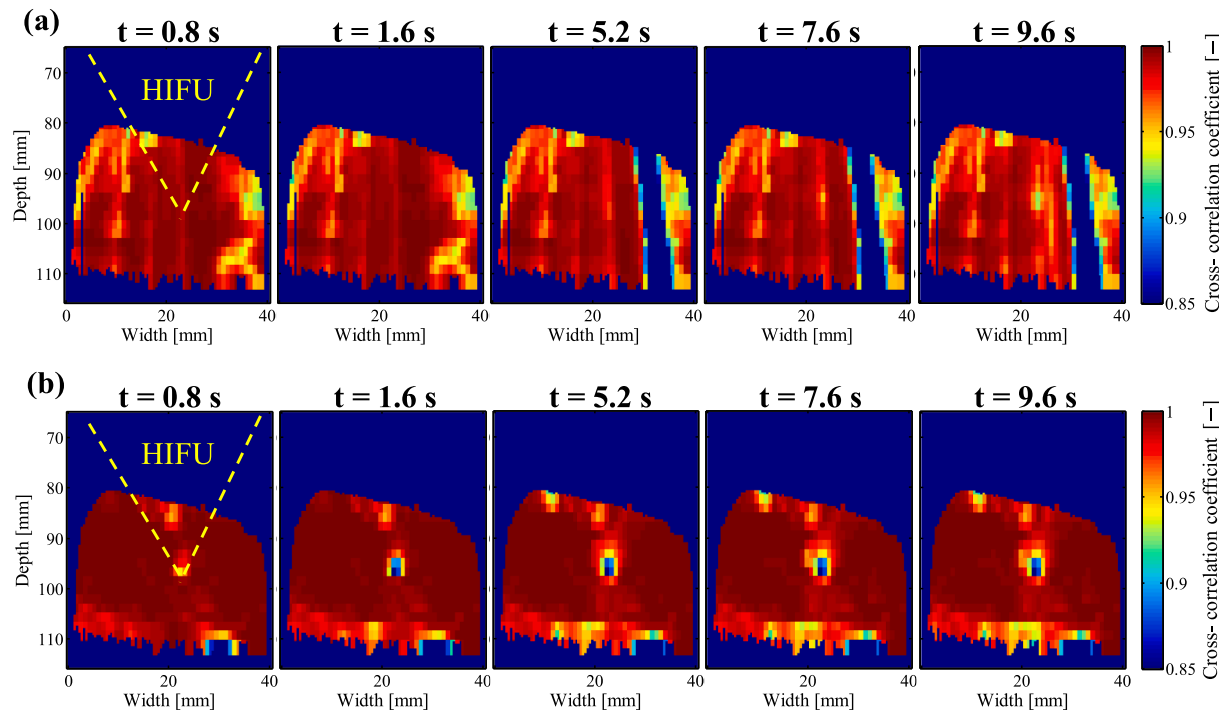


Fig. 9. Distributions of the correlation coefficient between the B-mode images in Fig. 8.

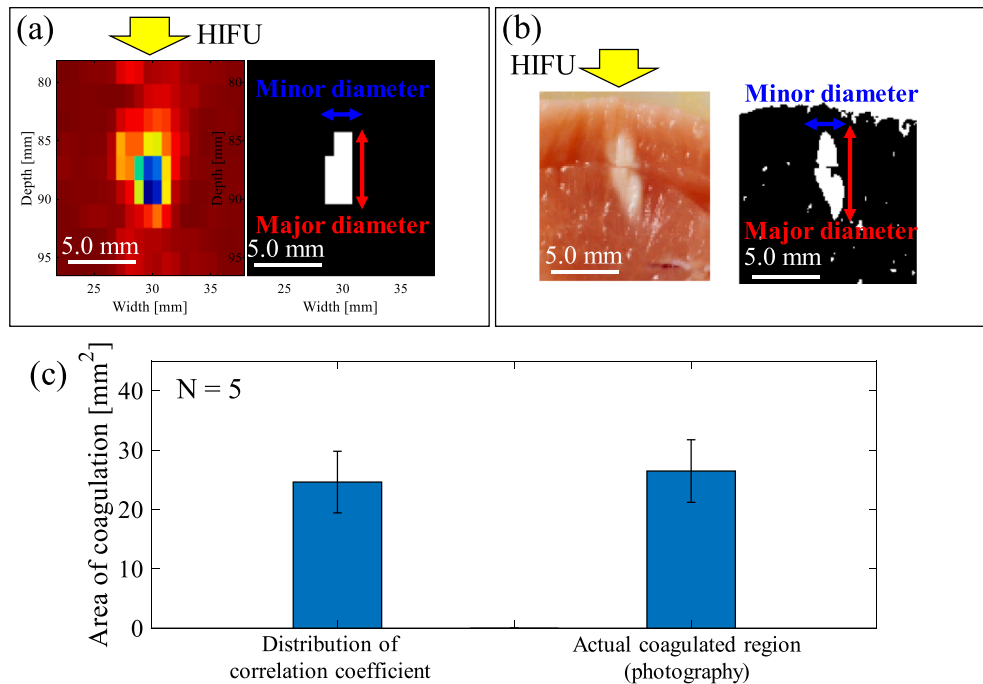


Fig. 10. (a) Binarized distribution of correlation coefficient in the focal region; (b) binarized photography of a cross-sectional slice of tissue sample after the HIFU exposure; and (c) comparison of the area of coagulation estimated from the binarized distribution of correlation coefficient and photographs.

here, the area of coagulation is assumed to be a ellipse and the axis of symmetry is parallel to the propagation of HIFU. Fig. 10(c) shows the comparison of the area of coagulation estimated from the binarized distribution of correlation coefficient and the photographs. The area of coagulation that is estimated from the binarized distribution of correlation coefficient and photographs were $24.6 \pm 5.19 \text{ mm}^2$ and $26.5 \pm 5.27 \text{ mm}^2$, respectively as shown in Fig. 10 (c).

Fig. 11 shows the noise-reduction level during HIFU exposure in

terms of the fundamental to third harmonic components of the HIFU. It was averaged for 5 samples and plotted against the HIFU exposure time. The noise reduction level of the fundamental, second, and third harmonic components was 50, 2, and 28 dB, respectively.

Fig. 12 shows (a) a signal level along a depth of 75 mm in the water region (dashed line) and (b) time and sample-averaged signal levels along a depth of 75 mm. Here, the signal level was normalized by the maximum value in the B-mode image at each time. As shown in Fig. 12,

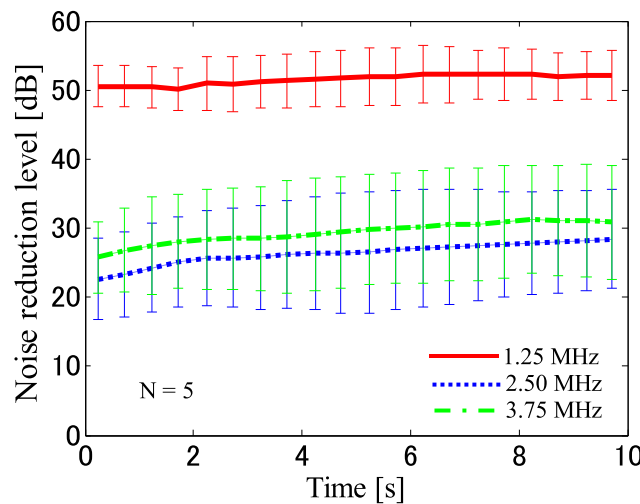


Fig. 11. Noise reduction level during HIFU exposure (“Heating only”) in terms of the fundamental to third harmonic components of the HIFU.

the signal levels in the water region (without the pulse responses) were less than about –40 dB, which indicates that almost all HIFU noises in the B-mode images were eliminated.

3.2. The “Trigger HIFU” sequence

Fig. 13 (a) and (b) show the B-mode images during the “Trigger HIFU” sequence before and after HIFU noise reduction, respectively. The HIFU was also irradiated above in a downward direction. The reference RF signals used to estimate the CW response were those also corresponding to the depth of 70 mm in the B-mode images. The tissue image is seen well in **Fig. 13** (b) after HIFU noise reduction. The HIFU noise was not completely eliminated in the rasters running through the focal region of HIFU, probably due to the cavitation bubbles seen in the image. In contrast, tissue image during HIFU exposure is also almost entirely

contaminated with HIFU noise in **Fig. 13** (a).

In the case of the “Trigger HIFU” sequence, the coagulation region was estimated using the B-mode images after noise reduction because the transient signals of cavitation bubbles and uneliminated noises in the rasters running through the focal region of HIFU have affected the distribution of the correlation coefficient and become distorted. **Fig. 14** (a) shows a binarized noise-reduced B-mode image in the focal region where the region which is more than –6 dB from the maximum brightness in the B-mode images was kept as a white region. **Fig. 14** (b) shows the binarized photographs of a cross-sectional slice of tissue sample after HIFU exposure. “Major diameter” and “Minor diameter” were defined from the binarized images and the area of coagulation was estimated like the case of the “Heating only” sequence. **Fig. 14** (c) shows the comparison of the area of coagulation estimated from the binarized distribution of noise-reduced B-mode image and photograph. The area of coagulation estimated from the binarized B-mode image and photographs were $35.7 \pm 7.50 \text{ mm}^2$ and $31.1 \pm 5.66 \text{ mm}^2$, respectively as as shown in **Fig. 14** (c).

Fig. 15 also shows the noise reduction level in terms of the fundamental to third harmonic components of the HIFU. It was averaged for 5 samples. The noise reduction level of the fundamental, second, and third harmonic components was 48, 24, and 26 dB, respectively.

Fig. 16 shows (a) a signal level along a depth of 75 mm in the water region (dashed line) and (b) time and sample averaged signal levels along a depth of 75 mm. Here, the signal level was normalized by the maximum value in the B-mode image at each time. As shown in **Fig. 16** (b), the noise was not only reduced in the focal region (cavitation generated area) but also in the scanning line running through the HIFU focal zone (width = 18–26 mm) unlike with the “Heating only” sequence. The remaining noise level in the water region was from –35 to –20 dB, which was 5 to 20 dB larger than that of the noise-reduced region such as areas in the water without tissue signals.

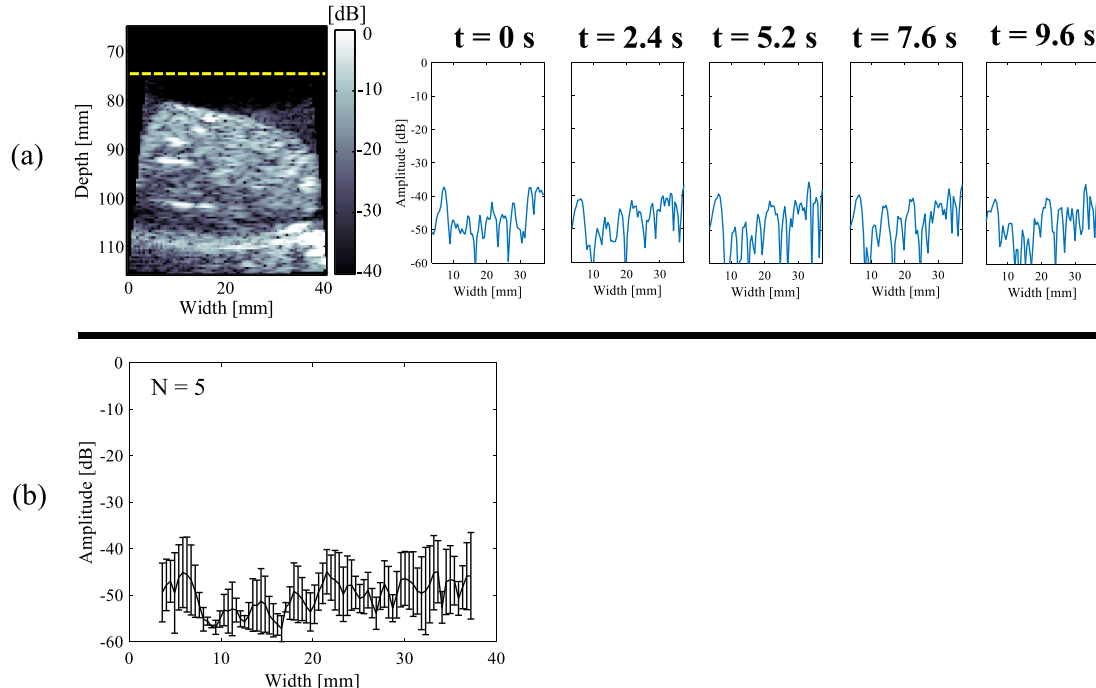


Fig. 12. (a) A signal level along a depth of 75 mm in the water region (dashed line) and (b) Time and sample-averaged signal levels along a depth of 75 mm in the “Heating only” sequence.

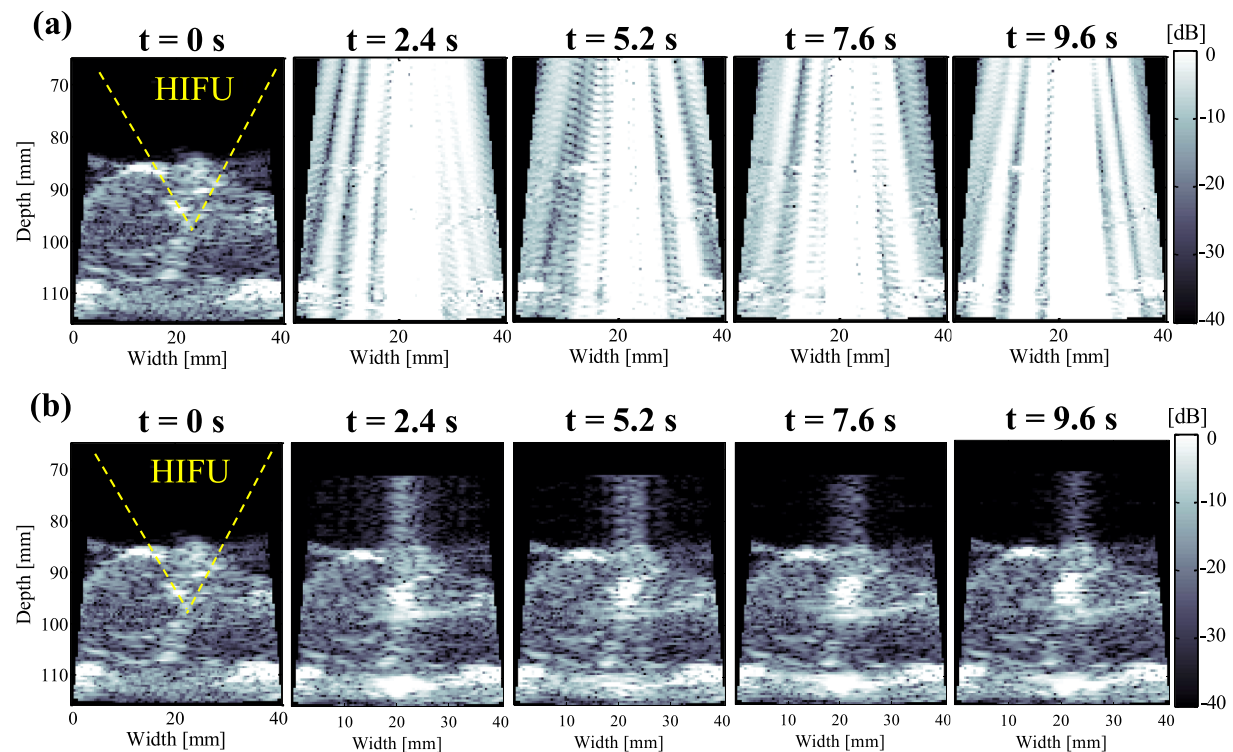


Fig. 13. B-mode images during the “Trigger HIFU” sequence, (a) before and (b) after HIFU noise reduction.

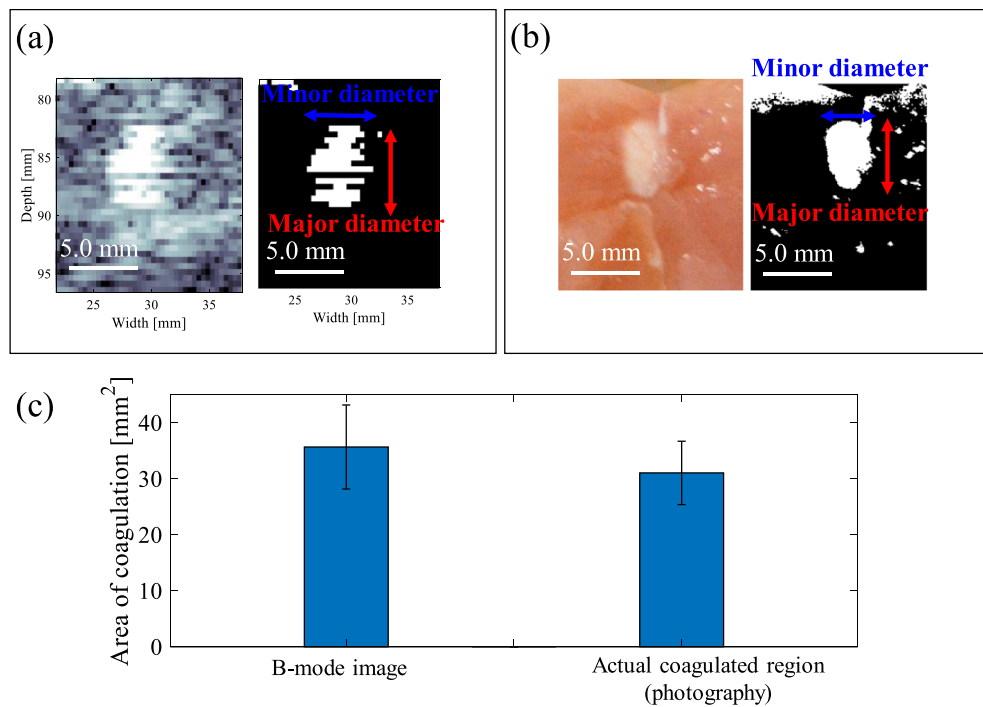


Fig. 14. (a) Binarized noise-reduced B-mode image in the focal region; (b) binarized photography of a cross-sectional slice of tissue sample after the HIFU exposure; and (c) comparison of the area of coagulation estimated from the binarized distribution of the correlation coefficient and photographs.

4. Discussion

4.1. The “Heating only” sequence

Fig. 8 shows that the proposed method can eliminate practically all HIFU noise while keeping the echo signals intact even when the imaging

beam is approximately parallel to the HIFU beam, although the RF signals received by the imaging probe may have HIFU components at higher amplitudes and the pulse echo RF signals can more likely be modulated by the HIFU radiation force than the perpendicular set up used in our preliminary study [24]. Truly real-time ultrasonic monitoring of HIFU treatment without intermission for HIFU exposure proves

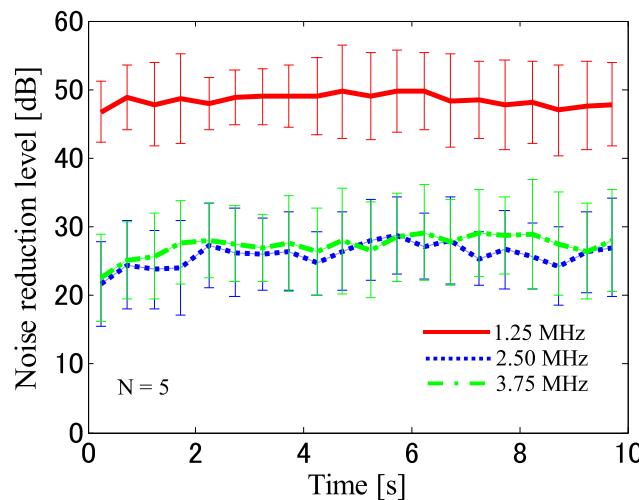


Fig. 15. Noise-reduction level during HIFU exposure ("Trigger HIFU") in terms of the fundamental to third harmonic components of the HIFU.

to be possible in a practical HIFU set-up. HIFU-induced coagulation was successfully detected using the correlation maximum distribution derived from the B-mode images after applying the proposed HIFU noise reduction method. The coagulation region estimated from the distribution of the correlation coefficient was compared with the actual coagulation region quantitatively by using binarized images as shown in Fig. 10. The size of the decorrelated area near the HIFU focus with a correlation coefficient less than 0.95 was about the same as the actual size of the treated region as shown in Fig. 10.

In these experiments, a correlation coefficient of 0.95 was set as a threshold to estimate the coagulation region in the distributions of the correlation coefficient. The estimated region (decorrelated area) was matched well to the actual coagulation region after HIFU exposure.

However, the setting threshold of the correlation coefficient (0.95) might not be applicable to all clinical practices. Further investigation is needed to investigate a way to decide the threshold appropriately through the experiments using various tissue samples such as liver and fat and setting several intensities of HIFU.

The tissue motion was not detected by calculating the displacement between the first and last B-mode images (RF1 and RF250 in Fig. 3) during HIFU exposure in all 5 samples, unlike with the results of the previous studies [22,23]. This is thought to be because the tissue was exposed to HIFU without intermission for ultrasound imaging and HIFU radiation force was applied to the tissue constantly during HIFU exposure. As described in the previous study [22,23], the small displacement (less than 125 μm) occurred approximately from 5 to 35 ms after the HIFU exposure ceased. Therefore, it is said that the motion-compensated algorithm to estimate the coagulation region was not absolutely necessary in a quasi-static case without HIFU intermission such as with these experiments. However, the unexpected tissue motion in the imaging plane can be caused by breathing and heartbeats in a real clinical treatment, although the target tissue is exposed to HIFU without intermission. So, the motion-compensated algorithm should be effective in the real clinical case. In the current setup, a maximum displacement of ± 0.9 and ± 1.75 mm in the axial and lateral directions can be tracked using two B-mode images and the fastest motion of ± 2.25 mm/s and ± 4.38 mm/s in the axial and lateral directions because the time between two B-mode images to estimate the coagulation region was 400 ms as described in Section 2.5.

The motion-compensated algorithm has to be applied to the bi-plane imaging using two 1-D array probes or three-dimensional (3-D) imaging using a 2-D array probe in case that possible changes in HIFU radiation force and breathing would induce an out-of-plane motion.

If HIFU exposure had been intermittent, an expected motion induced by the change in radiation force could have been much greater and affected the distribution of the correlation coefficient. This is also a great advantage of the proposed method that requires no HIFU intermission

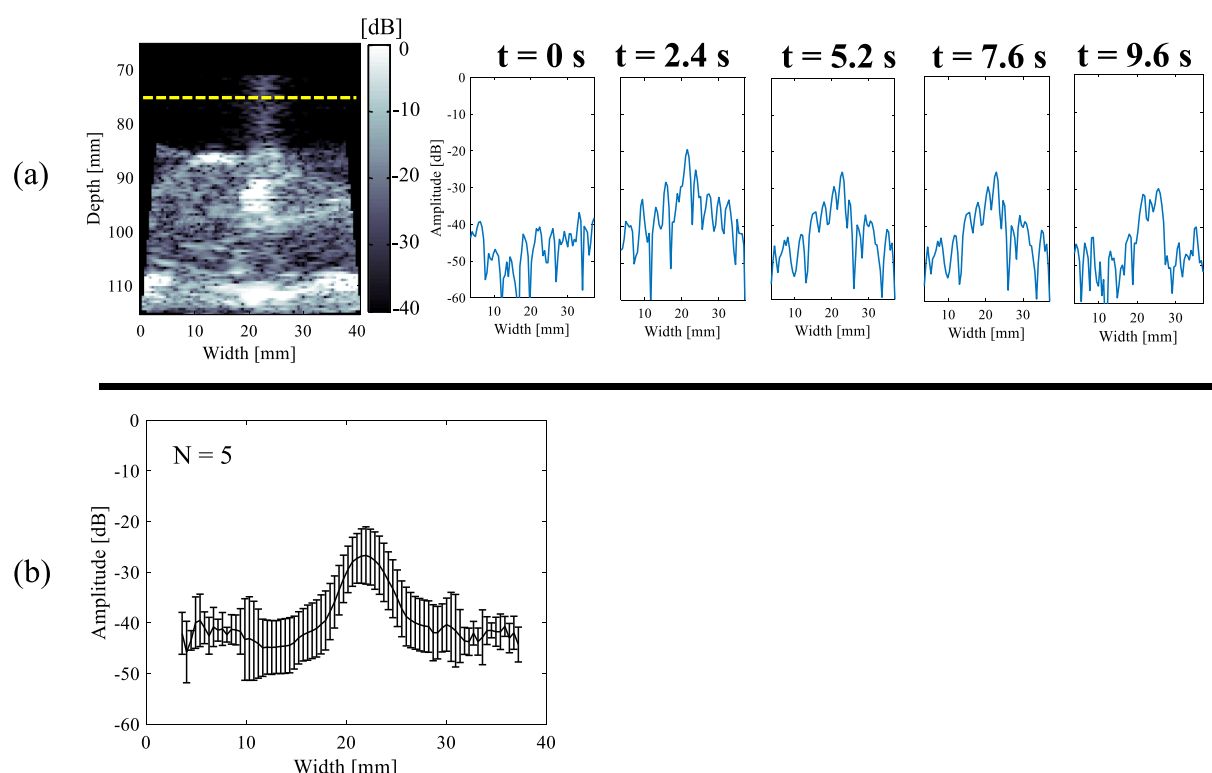


Fig. 16. (a) A signal level along a depth of 75 mm in the water region (dashed line) and (b) time- and sample-averaged signal levels along a depth of 75 mm in the "Trigger HIFU" sequence.

for imaging.

The noise-reduction level shown in Fig. 11 was larger than that of the preliminary study [24] where HIFU was irradiated perpendicular to the direction of the imaging pulse. This is because the RF signals contained higher amplitudes of HIFU noise due to the smaller backscattering angles [24].

4.2. The “Trigger HIFU” sequence

The HIFU noise was almost completely eliminated, and the generation of cavitation bubbles can be detected as shown in Fig. 13. Although a small amount of noise remained uneliminated in the scanning line running through the HIFU focal zone as seen in Fig. 13 (b), this result suggests that it is possible to monitor tissue changes using this proposed method even with a nonlinear transient response of the cavitation bubbles. The high brightness region due to cavitation at the HIFU focus was focused on the B-mode images as seen in Fig. 13.

The cross-correlation algorithm could not be used to estimate the coagulation region in the “Trigger HIFU” sequence because the signals of the cavitation bubbles and uneliminated noises in the scanning line running through the HIFU focus were transient and affects the distribution of the correlation coefficient. Therefore, the coagulation region was estimated by taking the high brightness region, which is more than -6 dB of the maximum brightness in the B-mode images, and quantitatively compared with the actual treated region using binarized images as shown in Fig. 14. The estimated area of coagulation was about the same as the actual size of the treated region although the estimated area was a little larger than the actual one because the estimated area included the high brightness pixels of uneliminated noises around the HIFU focus. The aspect ratio of the coagulated region was smaller than that of the “Heating only” sequence, which is probably because the cavitation-enhanced heating was more localized than heating by heating exposure alone.

The difference in the maximum brightness around the HIFU focus in B-mode images between “Heating only” and “Trigger HIFU” sequences was also investigated. Fig. 17(a) and (b) show that the B-mode images around the HIFU focus after noise reduction in the “Heating only” and

“Trigger HIFU” sequences. Fig. 17(c) shows the relative difference in the maximum brightness in B-mode images around the HIFU focus in both sequences, where the maximum brightness of “Heating only” sequences was set to zero. As shown in Fig. 17(c), the high brightness region of “Trigger HIFU” sequence due to the cavitation bubbles was 14.3 ± 0.94 dB larger than that of the “Heating only” sequence. It is said that the focal and coagulation region can be observed easily from the B-mode images after noise reduction without the cross-correlation algorithm in the “Trigger HIFU” sequence, which is also one of the advantages of the cavitation-enhanced HIFU exposure.

In this section, the reason that some noise remained uneliminated in the scanning line running through the area of cavitation in Fig. 13 (b) is discussed by comparing the cases of “Heating only” and “Trigger HIFU”.

In the proposed algorithm, it is assumed that the CW response to HIFU reaches its steady state within a few milliseconds [24] after the HIFU exposure has started to heat. The steady-state CW response can be estimated based on the RF signal in the time window where no imaging pulse response should be received. Subtracting the estimated CW response [$CW_{est}(t)$] from the RF signals should yield an imaging pulse response [$u(t)$] that is free from HIFU noise. The HIFU noise was practically completely eliminated in the case of the “Heating only” sequence, as shown in Fig. 4 (b) because this assumption is perfectly applicable to the case. However, this assumption does not perfectly hold true in the case of the “Trigger HIFU” sequence. This is because the “Trigger” pulse and the induced cavitation bubbles are transient, resulting in transient echo signals. Their characteristic time can be less than a millisecond.

To support this hypothesis, a 1-D normalized cross-correlation was performed using the original and estimated HIFU response acquired $10\ \mu s$ after the reference signal to estimate the CW response. The duration of RF signal to calculate the 1-D normalized cross-correlation was $15\ \mu s$. Fig. 18 (a) shows an example of the calculation of the 1-D normalized cross-correlation using the original and estimated HIFU response in the “Heating only” sequence. Fig. 18 (b) and (c) shows the time- and sample-averaged correlation coefficient in each element between the original and estimated CW response in the “Heating only” and “Trigger HIFU” sequences, respectively. Fig. 18 (b) shows that the correlation coefficient equals one in all elements in the “Heating only” sequence, which indicates that the actual CW response could be estimated entirely using the RF signal in the time window without imaging pulse responses. On the other hand, the correlation coefficient was remarkably decreased in the center elements (from channel 30 to 60), which corresponds to the scanning line running through the HIFU focus in the “Trigger HIFU” sequence as shown in Fig. 18 (c). These results show that the CW response received in the center elements was mainly distorted by the transient cavitation effect in the HIFU focal region and the estimated CW response was deviated from the original CW response at an order of microseconds. These results also indicate that the cavitation bubbles induced in these experiments behaved like linear scatterers that strongly reflect the ultrasonic signal right back to the phased-array probe (parallel to the axial direction of HIFU) because the reflected CW response in the center elements was mainly affected and distorted by the cavitation bubbles in the HIFU focal zone.

Based on these results, it is possible to monitor the state of oscillation (i.e., stable or inertial cavitation) and the behavior of the bubbles as scatterers (i.e., linear or nonlinear) during the “Trigger HIFU” sequence by analyzing the reflected CW response received in the elements. Further investigation is needed by changing the parameters such as the intensity and duration of the “Trigger” pulse or the sequence of HIFU exposure to clarify the relationship between the oscillation of HIFU-induced cavitation bubbles and the resulting HIFU response.

In the “Trigger HIFU” sequence, it is possible that the cavitation bubbles may be generated at the entry surface of the tissue. This is because the acoustic pressure of the “Trigger pulse” is large enough to cause cavitation bubbles at the surface due to the definite difference in acoustic impedances between the water and the tissue. However, it is thought that the cavitation bubbles were not generated at the surface of

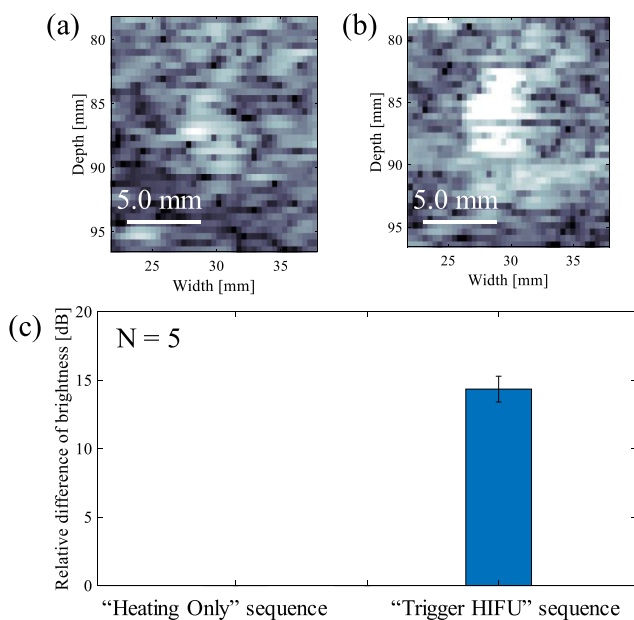


Fig. 17. B-mode images around the HIFU focus after noise reduction in the (a) “Heating only” and (b) “Trigger HIFU” sequences; (c) Relative difference of the maximum brightness in B-mode images around the HIFU focus in both sequences where the maximum brightness of “Heating only” sequences was set to zero.

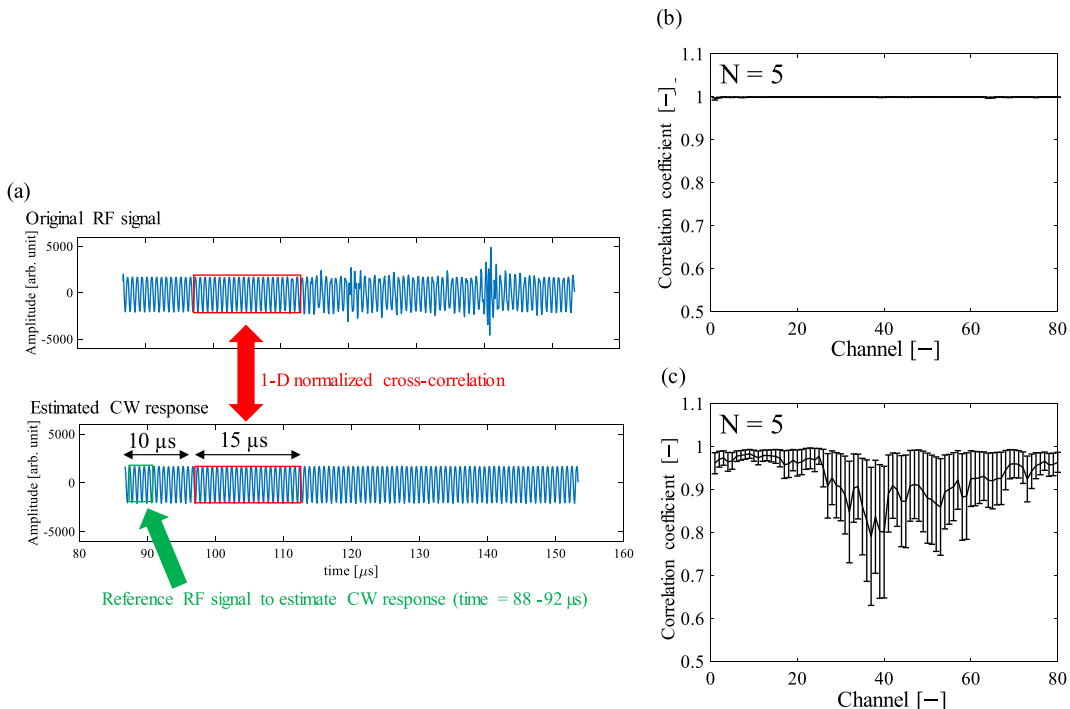


Fig. 18. (a) An example of the calculation of 1-D normalized cross-correlation using the original and estimated HIFU response in the “Heating only” sequence and the time and sample averaged correlation coefficient in each element between the original and estimated CW response in the case of (b)“Heating only” and (c)“Trigger HIFU” sequences, respectively.

the tissue in these experiments using 5 samples because the brightness, which is at the same level as the focal region, was not observed at the entry surface of the tissue. Few cavitation bubbles might be generated at the surface where small RF signals are reflected transiently. However, the effect of these signals on the noise reduction method is thought to be relatively small. The relationship between the cavitation bubbles at the surface of the tissue and the distortion of the estimated CW response has to be investigated by assigning different intensities and durations of the “Trigger pulse” to intentionally produce cavitation bubbles at the surface of the tissue.

Fig. 19 compares the power spectra of the RF signal after HIFU noise reduction 0.2, 2.2, 4.2, 6.2 and 8.2 s after the start of HIFU exposure in the case of (a) “Heating only” and (b) “Trigger HIFU” sequences. Here, the power spectra received by all elements (80 ch) over 7 time transmissions were averaged. These power spectra were acquired from the experiments of tissue samples as shown in Figs. 8 and 13. As shown in Fig. 19, there were sub-harmonic components and nonlinear interaction between the HIFU and the imaging pulse in the power spectra in the case of the “Trigger HIFU” sequence. It is thought that such noise was caused

by the chaotic and transient nature of the cavitation bubbles affecting CW response and becoming the components of uneliminated noise after HIFU noise reduction.

As shown in Fig. 15, the fundamental to higher harmonic components of HIFU noise in the “Trigger HIFU” sequence were reduced to a similar level as the “Heating only” sequence. In spite of the remaining HIFU noise, observation of cavitation bubbles was possible using the proposed method, suggesting that it is practically useful for monitoring the cavitation-enhanced HIFU treatment.

5. Conclusions

A novel filtering method to selectively eliminate HIFU noise components from RF signals for imaging, which is totally different from the conventional frequency-domain filter, was tested in a practical set-up. Unlike the preliminary test, the imaging probe was set inside the HIFU transducer. This set-up can make the RF echo signals more transient because the HIFU beam is almost parallel to the imaging beam. It is possible to detect tissue denaturation due to HIFU without an HIFU

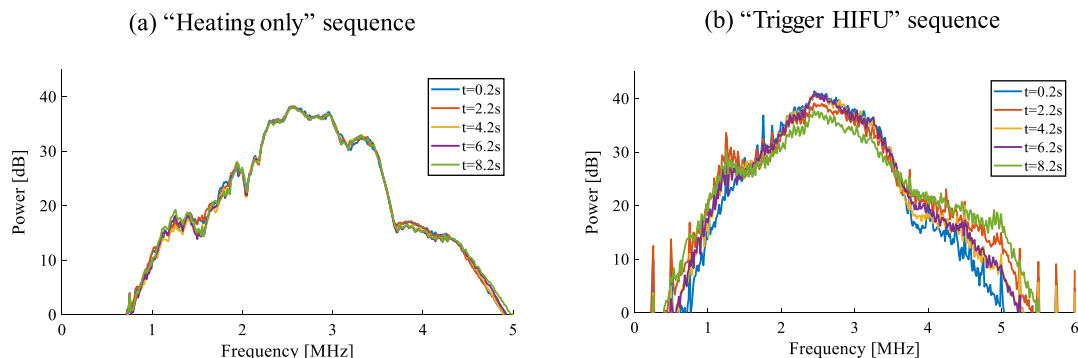


Fig. 19. Comparison of RF signal power spectra signal after HIFU noise reduction 0.2, 2.2, 4.2, 6.2, and 8.2 s after the start of HIFU exposure in (a) “Heating only” and (b) “Trigger HIFU” sequences.

intermission period, suggesting that the proposed method is practically useful for monitoring the tissue in real time in ultrasound-guided HIFU treatment.

The method was also applied to a cavitation-enhanced HIFU treatment, in which chaotic acoustic signals can be emitted by cavitation bubbles in the focal region of HIFU. HIFU noise was eliminated enough to observe cavitation bubbles generated during HIFU exposure. This demonstrated the robustness of the proposed method even in complex conditions.

Declaration of Competing Interest

The authors declare that they have no known competing financial interests or personal relationships that could have appeared to influence the work reported in this paper.

Acknowledgments

This work was supported by a Grant-in-Aid for Young Scientists (Grant Number 19K20725).

References

- [1] C.A. Linke, E.L. Carstens, L.A. Frizzell, A. Elbadawi, C.W. Fridd, Localized tissue destruction by high-intensity focused ultrasound, *Arch. Surg.* 107 (1973) 887–891.
- [2] J.C. Bamber, C.R. Hill, Ultrasonic attenuation and propagation speed in mammalian tissues as a function of temperature, *Ultrasound Med. Biol.* 5 (1979) 149–157.
- [3] P.M. Corry, K. Jabboury, E.P. Armour, J.S. Kong, Human cancer-treatment with ultrasound, *IEEE Trans. Ultrason. Ferroelectr. Freq. Control* 31 (1984) 444–456.
- [4] J.E. Kennedy, G.R. Ter Haar, D. Cranston, High-intensity focused ultrasound: surgery of the future? *Br. J. Radiol.* 76 (2003) 590–599.
- [5] N.T. Sanghvi, F.J. Fry, R. Bihrl, R.S. Foster, M.H. Phillips, J. Syrus, Zaitsev A V and Hennige C W “Noninvasive surgery of prostate tissue by high-intensity focused ultrasound”, *IEEE Trans. Ultrason. Ferroelectr. Freq. Control* 43 (1996) 1099–1110.
- [6] G. Vallancien, E. Chartier-Kastler, M. Harouni, Focused extracorporeal pyrotherapy: Experimental study and feasibility in man, *Semin. Urol.* 11 (1993) 7–9.
- [7] A.H. Chan, V.Y. Fujimoto, D.E. Moore, R.W. Martin, S. Vaezy, An image guided high-intensity focused ultrasound device for uterine fibroids treatment, *Med. Phys.* 29 (2002) 2611–2620.
- [8] F. Wu, Z. Wang, W. Chen, J. Bai, H. Zhu, T. Qiao, Preliminary experience using high-intensity focused ultrasound for the treatment of patients with advanced stage renal malignancy, *J. Urol.* 170 (2003) 2237–2240.
- [9] F. Wu, Z. Wang, H. Zhu, Feasibility of US-guided high-intensity focused ultrasound treatment in patients with advanced pancreatic cancer: Initial experience, *Radiology* 236 (2005) 1034–1040.
- [10] H.E. Cline, K. Hyynnen, R.D. Watkins, W.J. Adams, J.F. Schenck, R.H. Ettinger, W. R. Freund, J.P. Vetro, F.A. Jolesz, Focused US system for MR imaging-guided tumor ablation, *Radiology* 194 (1995) 731–737.
- [11] H. Furusawa, K. Namba, S. Thomsen, F. Akiyama, A. Bendet, C. Tanaka, Yasuda Y and Nakahara H “Magnetic resonance-guided focused ultrasound surgery of breast cancer: reliability and effectiveness”, *J. Am. Coll. Surg.* 203 (2006) 54–63.
- [12] G. Ter Haar, D. Sinnett, I. Rivens, High-intensity focused ultrasound—a surgical technique for the treatment of discrete liver-tumors, *Phys. Med. Biol.* 34 (1989) 1743–1750.
- [13] R. Yang, K. Kopecky, F.J. Rescorla, C.A. Galliani, Wu E X and Grosfeld J L”, Sonographic and computedtomography characteristics of liver ablation lesions induced by high-intensity focused ultrasound”, *Invest. Radiol.* 28 (1993) 796–880.
- [14] G. Ter Haar, D. Sinnett, I. Rivens, High-intensity focused ultrasound - a surgical technique for the treatment of discrete liver-tumors, *Phys. Med. Biol.* 34 (1989) 1743–1750.
- [15] R. Yang, K. Kopecky, F.J. Rescorla, C.A. Galliani, E.X. Wu, J.L. Grosfeld, Sonographic and computedtomography characteristics of liver ablation lesions induced by high-intensity focused ultrasound, *Invest. Radiol.* 28 (1993) 796–801.
- [16] C. Simon, P. Vanbare, E.S. Ebbini, Two-dimensional temperature estimation using diagnostic ultrasound, *IEEE Trans. Ultrason. Ferroelectr. Freq. Control* 45 (4) (1998) 1088–1099.
- [17] R. Righetti, et al., Elastographic characterization of HIFU-induced lesions in canine livers, *Ultrasound Med. Biol.* 25 (7) (1999) 1099–1113.
- [18] E.E. Konofagou, et al., The temperature dependence of ultrasound-stimulated acoustic emission, *Ultrasound Med. Biol.* 28 (3) (2002) 331–338.
- [19] B.J. Fahey, et al., Acoustic radiation force impulse imaging of thermally- and chemically-induced lesions in soft tissues: preliminary ex vivo results, *Ultrasound Med. Biol.* 30 (3) (2004) 321–328.
- [20] J. Bercoff, M. Tanter, M. Fink, Supersonic shear imaging: A new technique for soft tissue elasticity mapping, *IEEE Trans. Ultrason. Ferroelectr. Freq. Contr.* 51 (2004) 396–409.
- [21] T. Shishitani, R. Matsuzawa, S. Yoshizawa, S. Umemura, Changes in backscatter of liver tissue due to thermal coagulation induced by focused ultrasound, *J. Acoust. Soc. Am.* 134 (2013) 1724–1730.
- [22] R. Matsuzawa, T. Shishitani, S. Yoshizawa, S. Umemura, Monitoring of Lesion Induced by High-Intensity Focused Ultrasound Using Correlation Method Based on Block Matching, *Jpn. J. Appl. Phys.* 51 (2012) 1–6.
- [23] S. Sasaki, R. Takagi, K. Matsuura, S. Yoshizawa, S. Umemura, Monitoring of high-intensity focused ultrasound lesion formation using decorrelation between high-speed ultrasonic images by parallel beamforming, *Jpn. J. Appl. Phys.* 53 (2014) 1–6.
- [24] R. Takagi, K. Goto, H. Jimbo, K. Matsuura, R. Iwasaki, S. Umemura, S. Yoshizawa, Elimination of therapeutic ultrasound noise from pre-beamformed RF data in ultrasound imaging for ultrasound-guided high-intensity focused ultrasound treatment, *Jpn. J. Appl. Phys.* 52 (2015) 1–6.
- [25] R. Takagi, S. Yoshizawa, S. Umemura, Enhancement of Localized Heating by Ultrasonically Induced Cavitation in High-intensity Focused Ultrasound Treatment, *Jpn. J. Appl. Phys.* 49 (2010) 1–4.
- [26] R. Takagi, S. Yoshizawa, S. Umemura, Cavitation Inception by Dual-Frequency Excitation in High-Intensity Focused Ultrasound Treatment, *Jpn. J. Appl. Phys.* 50 (2011) 1–5.
- [27] S. Umemura, S. Yoshizawa, R. Takagi, Y. Inaba, J. Yasuda, Enhancement of Focused Ultrasound Treatment by Acoustically Generated Microbubbles, *Jpn. J. Appl. Phys.* 52 (2013) 1–6.
- [28] R.G. Holt, R.A. Roy, Measurements of bubble-enhanced heating from focused, MHz-frequency ultrasound in a tissue-mimicking material, *Ultrasound Med. Biol.* 27 (2001) 1399–1412.
- [29] M.R. Bailey, L.N. Courte, O.A. Sapozhnikov, V.A. Khokhlova, G. ter Haar, S. Vaezy, X. Shi, R. Martin, L.A. Crum, Use of overpressure to assess the role of bubbles in focused ultrasound lesion shape in vitro, *Ultrasound Med. Biol.* 27 (2001) 695–708.
- [30] Y. Inaba, S. Yoshizawa, S. Umemura, Coagulation of Large Regions by Creating Multiple Cavitation Clouds for High-intensity Focused Ultrasound Treatment, *Jpn. J. Appl. Phys.* 49 (2010) 1–4.
- [31] Y. Inaba, T. Moriyama, S. Yoshizawa, S. Umemura, Ultrasonic Coagulation of Large Tissue Region by Generating Multiple Cavitation Clouds in Direction Perpendicular to Ultrasound Propagation, *Jpn. J. Appl. Phys.* 50 (2011) 1–7.
- [32] T. Moriyama, S. Yoshizawa, S. Umemura, Thermal Simulation of Cavitation-Enhanced Ultrasonic Heating Verified with Tissue-Mimicking Gel, *Jpn. J. Appl. Phys.* 51 (2012) 1–6.
- [33] K. Goto, R. Takagi, T. Miyashita, H. Jimbo, S. Yoshizawa, S. Umemura, Effect of controlled offset of focal position in cavitation-enhanced high-intensity focused ultrasound treatment, *Jpn. J. Appl. Phys.* 54 (2015) 1–4.
- [34] T.R. Gururaja, W.A. Schulze, L.E. Cross, R.E. Newham, B.A. Auld, Y.J. Wang, Piezoelectric Composite Materials for Ultrasonic Transducer Applications. Part I: Resonant Modes of Vibration of PZT Rod-Polymer Composites, *IEEE Trans. Sonics Ultrason.* 32 (1985) 481–498.
- [35] K. Moro, S. Yoshizawa, S. Umemura, Staircase-Voltage Metal-Oxide-Semiconductor Field-Effect Transistor Driver Circuit for Therapeutic Ultrasound, *Jpn. J. Appl. Phys.* 49 (2010) 1–4.